Parallel Pool Analysis of Transient Spectroscopy Reveals Origins of and Perspectives for ZnO Hybrid Solar Cell Performance Enhancement Using Semiconducting Surfactants

ARTICLE *in* JOURNAL OF PHYSICAL CHEMISTRY LETTERS · SEPTEMBER 2012

Impact Factor: 7.46 · DOI: 10.1021/jz3006207

THE JOURNAL OF PHYSICAL CHEMISTRY Letters

Letter

pubs.acs.org/JPCL

Parallel Pool Analysis of Transient Spectroscopy Reveals Origins of and Perspectives for ZnO Hybrid Solar Cell Performance Enhancement Using Semiconducting Surfactants

Michael Meister,[§,∥] Jason J. Amsden,[*,†,‡,∥,⊥] Ian A. Howard,[*,§,⊥] Insun Park,[‡] Changhee Lee,[†] Do Y. Yoon,[‡] and Frédéric Laquai[*,§,⊥]

[†]School of Electrical and Computer Engineering, Interuniversity Semiconductor Research Center and Center for Multiscale Energy System, Seoul National University, Seoul 151-744, South Korea

[‡]Department of Chemistry, Seoul National University, Seoul 151-747, Korea

[§]Max Planck Research Group for Organic Optoelectronics, Max Planck Institute for Polymer Research, D-55128 Mainz, Germany

Supporting Information

ABSTRACT: Recently, the performance of ZnO nanocrystals as an electron acceptor in a solar cell device was significantly increased by a semiconducting surfactant. Here we show, using transient absorption spectroscopy and a parallel pool analysis, that changes in the quantum efficiency of charge generation account for the performance variation among semiconducting-surfactant-coated, surfactant-coated, and uncoated ZnO nanoparticles. We demonstrate that even better surfactant design to suppress fast recombination could still lead to a further doubling of device efficiency.

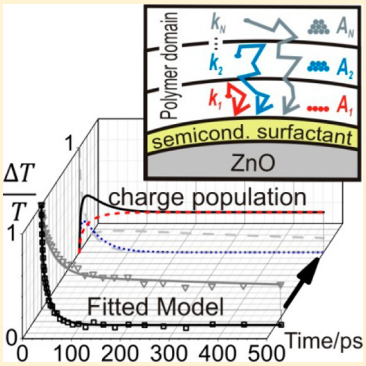

SECTION: Spectroscopy, Photochemistry, and Excited States

Semiconducting nanoparticles such as CdSe,[1] CdS,[2] PbS,[3,4] TiO_2,[5] and ZnO[6] offer alternatives to fullerenes as acceptors in bulk heterojunction photovoltaic devices. The semiconducting nanoparticles have several advantages such as high dielectric constant, tunable band gap (allowing tailoring of energy level alignment and optical absorption), and a wide selection of geometries including particles, rods, and tetrapods. In particular, ZnO is an attractive acceptor due to its nontoxicity, abundance, and ease of synthesis and processing.[7] Typically, bulk heterojunction devices that use conjugated polymers as donors and semiconducting nanoparticles as acceptors have had significantly poorer performance than analogous devices using fullerenes as acceptors. However, it was recently demonstrated that the performance of poly[2-methoxy-5-(3′,7′-dimethyloctyloxyl)-1,4-phenylene vinylene] (MDMO-PPV):ZnO solar cells could be significantly enhanced from ∼0.75 to ∼1.3% by coating the ZnO particles with a semiconducting surfactant,[8] which begins to approach the 2.5% efficiency typical of MDMO-PPV: C_{61}-butyric acid methyl ester (PCBM) devices.[9]

In this letter we demonstrate that time-resolved optical spectroscopy interpreted through a parallel-pool model can fully expose the changes in the device photophysics that lead to the increased efficiency, even when the rate constants are distributed rather than homogeneous. We determine which processes principally limit the internal quantum efficiency for cells prepared with semiconducting-surfactant-coated ZnO, ZnO coated with a nonsemiconducting surfactant, and uncoated ZnO and for each case with which approaches and by how much the internal quantum efficiency might still be increased.

The 3D mesostructure of a hybrid organic:inorganic bulk heterojunction using CdSe nanoparticles with short butylamine ligands has been fully characterized by electron tomography.[10] It was shown that in contrast with the intercalation and mixed phases that can occur in polymer:fullerene blends,[11] the nanoparticles tended to aggregate in the conjugated polymer matrix. This means that quenching of a polymer:nanocrystal blend exciton is strongly influenced by diffusion and therefore sensitively depends on the initial distance between the exciton and the interface. In addition, the quenching is affected by the probability that transfer occurs when an interface is reached. We expect these rates to vary between the three types of ZnO we prepared: One without surfactant, one with a recently developed long-chain semiconducting surfactant 2-(2-ethylhexyl)-1,3-dioxo-2,3-dihydro-1*H*-benzo[de]isoquinoline-6,7-di-

Received: May 16, 2012
Accepted: August 27, 2012
Published: August 27, 2012

carboxylic acid (BQ),[8] and one with a nonsemiconducting surfactant oleic acid (OA). In previous work, we observed that the dispersion of the nanoparticles drastically increases with the use of the surfactants, but the morphology is similar for both the semiconducting and nonsemiconducting surfactant, so differences in exciton quenching between the surfactants may be primarily influenced by a change in the probability of exciton quenching when the surfactant interface is reached.[8] Blend films of ∼100 nm thickness were prepared on quartz substrates with a 1:2 weight ratio of MDMO-PPV to ZnO for each ZnO type. For the surfactant-coated ZnO, the ZnO contained 3% by weight of the surfactant.

In Figure 1a, we present how we will approach the analysis of the time dependent, diffusion-influenced rate of exciton quenching using the sum of parallel pools. The net effective rate of exciton quenching can be represented by a sum of rates for excitons initially created in parallel population pools each with a unique characteristic exciton quenching rate k_i and population fraction A_i. These reaction rates need not be purely diffusion-limited as the k_i values can also account for a nonunity probability of charge transfer at the interface, which will likely be the case at least for the (OA)ZnO. Our parallel pool method works by analogy to our previous work on determining the phase-domain size in polymer:polymer blends.[12] We either select a set of physically reasonable k_i values and then allow the fractions of the population, the A_i values, to vary to give the best fit to the experimental data or we allow both the k_i values and A_i values to vary.[13] In either case, we can use them to calculate the average decay rate of the entire population as $\tilde{k} = (\sum_i A_i/k_i)^{-1}$. This average rate, $\tilde{k}$, can then be compared with other rates to determine quantitatively population evolutions and quantum efficiencies.

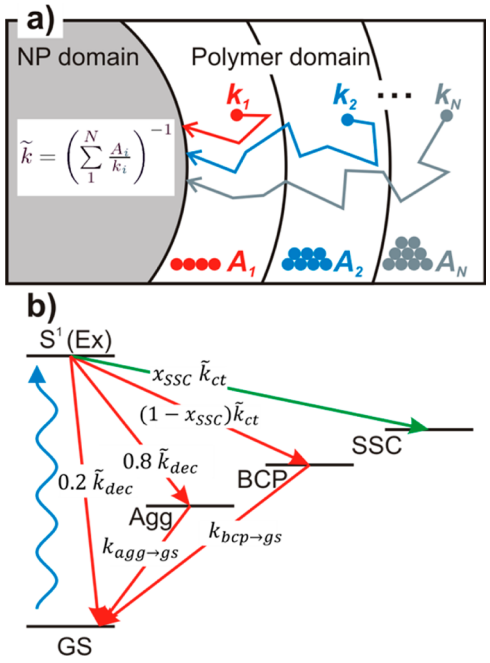

Figure 1. Panel a shows how the distributed rate of exciton quenching at nanoparticle:polymer interfaces can be represented by a sum of parallel population pools. Panel b shows the photophysical model used to fit the transient absorption kinetics of the MDMO-PPV:ZnO blend films. Ex: primary intrachain excitons; Agg: interchain aggregate states; BCP: bound charge pairs that lead to fast recombination to the ground state (GS); SSC: spatially separated free charges that do not recombine on the time scale of the experiment. k_x are rates related to single exponential decays, where x is indicating the transition it refers to; $\tilde{k}_x$ are parallel pool averages used to take into account the distributed or time-dependent rates. Here $x = dec$ denotes the depopulation of Ex due to recombination and energy transfer to aggregate, and $x = ct$ denotes the depopulation of Ex due to charge transfer. x_{SSC} is the fraction of exciton quenching by charge transfer that leads to spatially separated charges.

Our goal is to understand how the surfactant-induced changes affect the internal quantum efficiency of the photovoltaic blends. To achieve this, we will use the aforementioned parallel pool technique alongside the relevant photophysical model as shown in Figure 1b (which we develop and justify in the coming text) to fit the stimulated emission and photoinduced absorption transients measured with ultrafast pump−probe spectroscopy. Examples of the measured transient absorption data are shown in Figure 2 for the neat MDMO-PPV film and the MDMO-PPV:(BQ)ZnO film. The positive signal shown by the blue lines is due to stimulated emission of the exciton species. Because excitons are quenched by charge transfer in the blends, this signal becomes a negative charge-induced absorption. In the photoinduced absorption region shown by the red lines, the photoinduced absorptions of excitons, MDMO-PPV aggregates, and charges all play roles. A slight complication, observable in Figure 2b in the different decay of the red and blue lines, is that exciton quenching occurs even in neat MDMO-PPV films due to energy transfer to aggregate states in MDMO-PPV. We note that the presence of aggregate states in MDMO-PPV has been well-established in previous literature.[14−16] This means, though, that to characterize accurately the charge-transfer-induced exciton quenching, we must take into account this competing aggregate-induced quenching. To establish the rate of aggregate induced quenching, we will begin by examining the kinetics of the neat MDMO-PPV film.

Using a parallel pool model to account for the different rates of exciton quenching by energy transfer to aggregates, the evolution of the emissive exciton population in the neat material (normalized to the initial exciton concentration) can be expressed as $Ex_{neat}(t) = \sum_{i=1}^{N} A_i \exp(-k_{dec,i}t)$, where N is the number of subsets, A_i is the fraction of the total population that decays with the rate $k_{dec,i}$, and $\sum_{i=1}^{N} A_i = 1$. The population of aggregate states in the neat film is given by $Agg_{neat}(t) = (1 - PLQE) \times \tilde{k}_{dec}/(\tilde{k}_{dec} - k_{agg\rightarrow gs})[\exp(-k_{agg\rightarrow gs}t)] - Ex_{neat}(t))$, where $\tilde{k}_{dec}$ is the inverse of the weighted average decay lifetime of the exciton ($\tilde{k} = (\sum_i A_i/k_i)^{-1}$), and $k_{agg\rightarrow gs}$ is the monoexponential rate of aggregate decay to the ground state. The photoluminescence quantum efficiency (PLQE) of MDMO-PPV in film is ∼20%.[17] Making the assumption that aggregate formation is the primary nonradiative decay channel, the rate of aggregate formation is $\tilde{k}_{agg} = (1 - PLQE) \times \tilde{k}_{dec} = 0.8\tilde{k}_{dec}$. This assumption is justified by the fact that the PLQE is significantly lower in film than in solution. The normalized transient absorption of the neat material shown in Figure 3a can be fit simultaneously in the region of the stimulated emission (610−675 nm) and the photoinduced absorption (900−950 nm, using Origin 8.5, Originlab) with the equations $((\Delta T)/T)_{stim} = Ex_{neat}(t)$ and $((\Delta T)/T)_{pia} = Ex_{neat}(t) + r^{pia}_{Agg/Ex}Agg_{neat}(t)$, where $r^{pia}_{Agg/Ex}$ represents the ratio between the cross-section of the aggregate and the exciton in the photoinduced absorption region. The equation for the stimulated emission region can neglect the influence of aggregates, as we observe that the signal in this region decays

dx.doi.org/10.1021/jz3006207 | J. Phys. Chem. Lett. 2012, 3, 2665−2670

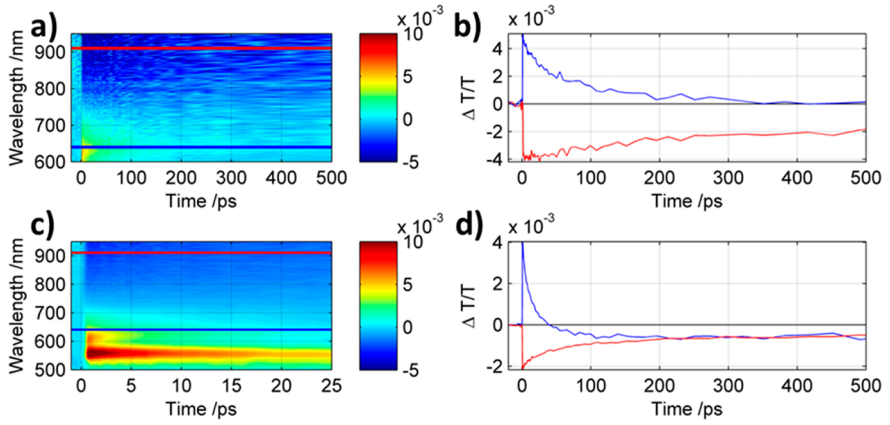

Figure 2. Representative transient absorption data of neat MDMO-PPV (a,b) and MDMO-PPV:(BQ)ZnO blend (c,d). Positive $\Delta T/T$ signals (stimulated emission and absorption bleach) are shown from cyan to red, whereas negative signals (photoinduced absorptions) are shown in blue. Panels a and b show the stimulated emission (600−700 nm, blue line) and photoinduced absorption (700−900 nm, red line) in the neat polymer. The stimulated emission decays more quickly than the photoinduced absorption, indicating, in accordance with previous literature, that dark aggregate states play a role alongside emissive excitons in the neat material and must be taken into account. Panel c shows the absorption bleach (long-lived positive signal centered at 550 nm), the quenched stimulated emission (600−700 nm, blue line), and photoinduced absorption (700−900 nm, red line) in the semiconducting surfactant blend. The efficiency of charge generation will be determined from the stimulated emission quenching, and the alteration of the photoinduced absorption kinetics examples of which are shown in panel d.

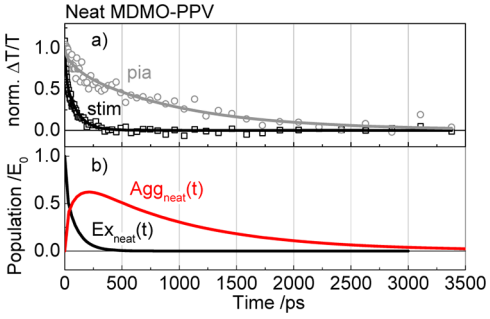

Figure 3. (a) Absorption transients of a neat MDMO-PPV film in the stimulated emission region 610−675 nm (black rectangles) and the photoinduced absorption region 900−950 nm (gray circles) along with a fit (solid lines) according to the model, as described in the text. (b) Population evolutions of primary intrachain excitons ($Ex_{neat}(t)$) and interchain aggregate states ($Agg_{neat}(t)$) as derived from the fit.

to zero by 300 ps, indicating that the cross-section of the aggregates is negligible in this wavelength range. Taking two distinct values for $k_{dec,i}$ ($k_{dec,1} = 1 \times 10^{11}$/s and $k_{dec,2} = 1 \times 10^{10}$/s) leads to the parameters shown in Table 1 and the lines shown in Figure 3a. Adding further population subsets did not improve the fitting. In Figure 3b, the extracted population evolutions of excitons and aggregates are shown.

Having established the rate of exciton quenching by transfer to aggregates, we can now examine the data from the blends to examine exciton quenching due to charge transfer. The normalized kinetics of the stimulated emission and photoinduced absorption regions are shown for each blend in the first row of Figure 4. In the stimulated emission region, the signal now becomes negative after a given time due to the non-negligible induced absorption of charges in this wavelength range. The photoinduced absorption now becomes a super-

Table 1. Parameters Determining Exciton Quenching by Energy Transfer to Aggregate States Extracted from Fitting of the Neat-Film-Stimulated Emission and Induced Absorption

parameter	neat fit values
A_1	0.326 ± 0.027
$k_{dec,1}/ps^{-1}$	0.1 fixed
A_2	0.674 ± 0.016
$k_{dec,2}/ps^{-1}$	0.01 fixed
$k_{agg\rightarrow gs}/ps^{-1}$	(1.04 ± 0.06)x10^{-3}
$r^{pia}_{Agg/Ex}$	0.907 ± 0.018

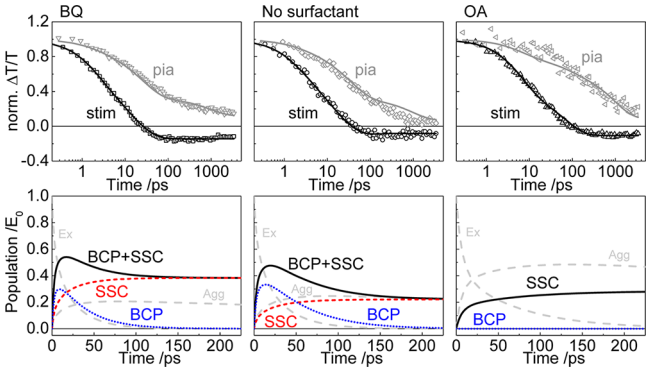

Figure 4. Kinetics of stimulated emission and photoinduced absorption for MDMO-PPV:ZnO blends with the three different surfactants BQ, no surfactant, and OA (upper panels, from left to right). The data are shown as dots along with the fitted curves (solid lines) derived from the model depicted in Figure 1b and described in the text. The lower panels show the population kinetics as obtained from the fitted model for the bound charge pair (BCP, dotted blue lines), the free spatially separated charges (SSC, dashed red lines), and the sum of both accounting for all charges created (solid black lines) for the three ZnO conformations. Populations of excitons (Ex) and aggregate states (Agg) are shown as gray dashed lines. BQ exhibits the highest splitting efficiency and OA exhibits the lowest along with a very low fraction of BCPs, whereas the particles without surfactant have the largest amount of BCPs and a similar splitting efficiency as OA.

dx.doi.org/10.1021/jz3006207 | J. Phys. Chem. Lett. 2012, 3, 2665−2670

position of signals originating from excitons, aggregates, and charges. To describe both wavelength regions in a single fit with shared parameters, a fast charge recombination channel has to be introduced. Without this channel, the photoinduced absorption and the stimulated emission regions of (BQ)ZnO and ZnO could not be described satisfactorily in the first few hundred picoseconds. This fast charge recombination component leads us to postulate that two populations of charges can be created. One, which we name bound charge pairs (BCPs), can undergo fast recombination, likely because the electron remains trapped on the surface of the nanoparticle or perhaps on the semiconducting surfactant. The other population, which we name spatially separated charges (SSCs), cannot decay on the nanosecond time scale because the charges achieve a significant enough initial separation that they no longer influence one another. We will examine the recombination of these free charges later and find that it occurs much more slowly on the time scale of tens of microseconds.

On the basis of the above qualitative observation regarding fast charge recombination, we introduce the factor x_{SSC} to represent the fraction of exciton quenching by charge transfer that leads to SSCs. (See Figure 1b.) For (OA)ZnO, the decay of the photoinduced absorption can be entirely explained by decay of the aggregate pool to the ground state with the rate previously determined in the neat film. (See Figure S4 in the Supporting Information.) Constraining x_{SSC} to 1 for (OA)ZnO is thus a reasonable assumption, whereas for the other two samples, it remains a fitting parameter. Leaving x_{SSC} a free parameter for (OA)ZnO results in over-parametrization and strong cross-correlations without improving the fit, justifying our constraint to the simpler model in this case. With this total model as shown in Figure 1b, the rate equations can be written for each state as:

$$Ex_{blend}(t) = Ex_{neat}(t) \sum_{M}^{i=1} C_i \exp(-k_{ct,i}t)$$

$$Agg_{blend}(t) = \frac{\tilde{k}_{agg}}{\tilde{k}_{dec} + \tilde{k}_{ct} - k_{agg\rightarrow gs}}(\exp(-k_{agg\rightarrow gs}t) - Ex_{blend}(t))$$

$$BCP(t) = \frac{(1 - x_{SSC})\tilde{k}_{ct}}{\tilde{k}_{dec} + \tilde{k}_{ct} - k_{bcp\rightarrow gs}}(\exp(-k_{bcp\rightarrow gs}t) - Ex_{blend}(t))$$

$$SSC(t) = \frac{x_{SSC}\tilde{k}_{ct}}{\tilde{k}_{dec} + \tilde{k}_{ct}}(1 - Ex_{blend}(t))$$

Exciton quenching due to charge transfer is diffusion-limited and analogous to the quenching through aggregates described by a multiexponential with subrates $k_{ct,i}$ and their weighting C_i. The transient absorption signals in the stimulated emission and absorption region can be expressed as:

$$\left(\frac{\Delta T}{T}\right)_{stim} = Ex(t) + r^{stim}_{CT/Ex}(BCP(t) + SSC(t))$$

$$\left(\frac{\Delta T}{T}\right)_{pia} = Ex(t) + r^{pia}_{Agg/Ex}Agg(t) + r^{pia}_{CT/Ex}(BCP(t) + SSC(t))$$

where $r^{stim}_{CT/Ex}$ and $r^{pia}_{CT/Ex}$ represent the ratios between the cross-sections of charges and excitons in the stimulated emission and photoinduced absorption region, respectively. All parameters obtained from the neat fit were adopted as fixed parameters. To obtain the most accurate parameter set possible, the stimulated emission together with the photoinduced absorption kinetics were fit at the same time for all three samples. Global variables, like the cross-section ratios, were shared across this global fit to the six data sets. Two subsets ($M = 2$) were sufficient to describe the CT-creation; adding further subsets did not improve the fitting. Further details of the fitting alongside a full table of extracted parameters with uncertainties are given in the Supporting Information. The results of the fitting are shown in the upper part of Figure 4. In the lower part, the evolution of the excited-state populations for each sample extracted from the global fitting is shown. Importantly, we can calculate the probability that a given absorbed photon results in SSCs for each sample as $\eta_{SSC} = x_{SSC}\tilde{k}_{CT}/(\tilde{k}_{dec} + \tilde{k}_{CT})$. We compare this probability with the internal photon conversion efficiency measured in the device structure in Table 2.

Table 2. Charge Separation Factors Extracted from the Fitting

sample	k_{ct}^{-1}/ps	x_{SSC} [a]	η_{SSC} [b]	IPCE
(BQ)ZnO	28 ± 7	0.51 ± 0.11	0.38 ± 0.06	0.44
ZnO	37 ± 7	0.31 ± 0.06	0.22 ± 0.04	0.29
(OA)ZnO	178 ± 48	1[c]	0.28 ± 0.05	0.27

[a] x_{SSC} is the portion of spatially separated charges of all excitons undergoing charge transfer. [b] η_{SSC} is the efficiency of free charge generation extracted from the fitting of the optical spectroscopy. [c] Parameter x_{SSC} of OA was fixed as explained in the text.

The exciton splitting efficiency obtained from the fitting roughly follows the trend of the incident photon to electron conversion efficiency (IPCE) data with the (BQ)ZnO having significantly more SSC generation and also a correspondingly higher IPCE. We note that although we would expect the SSC generation efficiency to be higher than the IPCE, the opposite is observed for ZnO and (BQ)ZnO. However, the IPCE was measured at the built-in field, whereas the spectroscopically determined SSC generation efficiency was measured in the absence of field. A slight field dependence of the SSC generation efficiency (x_{SSC}) would be physically reasonable and explain the underestimation of the quantum efficiency by the spectroscopic measurement in the ZnO and (BQ)ZnO samples.

The cause of the high η_{SSC} in the (BQ)ZnO is due to a fast effective rate of exciton quenching by charge transfer, which can be physically explained by the surfactant creating a good dispersion of ZnO nanocrystals in the polymer matrix and the probability of dissociation for an exciton reaching an interface remaining high.[18] Upon looking at the evolution of the total charge population, we see that it peaks at ~55% around 25 ps after photoexcitation and that the efficiency of SSC generation would be over 60% if x_{SSC} were unity in this sample. In terms of device performance, we see that suppressing the formation of quickly recombining trapped charges could double the efficiency of (BQ)ZnO, and doing this in combination with increasing the rate of exciton quenching by charge transfer so that it was much faster than aggregate formation could increase the efficiency by a factor of 3. So, significant room for

dx.doi.org/10.1021/jz3006207 | J. Phys. Chem. Lett. 2012, 3, 2665−2670

improvement remains for the quantum efficiency even in the most efficient (BQ)ZnO sample.

The ZnO sample has a slightly slower average rate of exciton quenching by charge transfer, but the rough similarity with the (BQ)ZnO sample suggests that the dispersion of the nanoparticles in terms of its effect on exciton quenching by charge transfer is not very different between the samples. Given that the morphology shown in ref 8 shows a less-dispersed structure for the uncoated ZnO, it is possible that the charge transfer itself is more effective, as no barrier between ZnO and polymer exists. If x_{SSC} were unity for the ZnO sample, then η_{SSC} would be tripled to a value over 60%. Therefore, our analysis shows that it is not the poor phase separation in the uncoated ZnO samples that is reducing quantum efficiency due to poor exciton quenching but rather that the majority of charges formed by exciton quenching quickly recombine in the absence of a surfactant. This could be due to a high number of surface states in ZnO,[19] leading to fast recombination of trapped charges.

The (OA)ZnO sample has a very much slower effective rate of exciton quenching by charge transfer. Because the OA surfactants do not negatively affect the dispersion of the nanocrystals in the polymer, we hypothesize that the presence of the bulky nonconjugated surfactant introduces a significant tunneling barrier to electron transfer for an exciton reaching the interface and therefore significantly reduces the probability that electron transfer occurs. This means that an exciton could have multiple encounters with the interface without being quenched by charge transfer. The consequence of this slow quenching by charge transfer is that a significant fraction of the exciton population decays into the aggregate state. It is worth noticing that the long chains of the surfactant could also influence the ordering of the polymer altering the exciton diffusion and polymer aggregation.[20,21] However, an advantage of the long inactive surfactant is that if charge transfer does occur, then there is negligible charge recombination on the short time scale. In contrast with the other samples, all quenching by charge transfer leads to free charges. This indicates that the long surfactant is effective in passivating the nanoparticle surface and hindering recombination but that this advantage is overwhelmed by its suppression of the charge-transfer rate.

Finally, to investigate the recombination of SSCs, Figure 5 shows the kinetics of the charge-induced absorption on the time scale of 500 ps to 20 μs. The recombination of free charges in all three cases is very slow. The free carrier lifetime is significantly longer than in PCBM for all ZnO samples, in agreement with previous studies,[22] suggesting that free carrier recombination competing with extraction may not play a significant role in reducing the quantum efficiency of these samples. This is consistent with our previous observation that the efficiency of free charge generation and the internal quantum efficiency were roughly similar. Therefore, we can conclude for all of these samples that the primary quantum efficiency loss mechanisms were the previously discussed limitations of SSC formation.

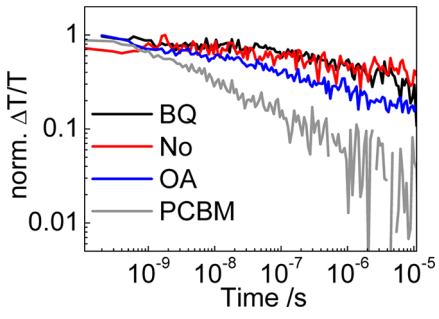

Figure 5. Long-time recombination kinetics of the different blends monitored at the photobleach. With PCBM, recombination is much faster. The ZnO blends exhibit a slower recombination that is in all three cases similar. Only OA has a slightly faster recombination.

In conclusion, our work highlights the importance of continuing to work on nanoparticle surfactant design and synthesis because with the aid of surfactants nanoparticle acceptors should be able to rival the efficiency of fullerenes in bulk heterojunction solar cells. The key functionality that the surfactant must enable appears to be the suppression of fast recombination while not hindering the efficient quenching of excitons by charge transfer.

Along this line, Sargent et al. recently achieved 6% power conversion efficiency using nanocrystal-based inorganic depleted-heterojunction solar cells based on the development of new atomic ligands that passivated surface states while introducing only minimal barriers to transport.[23] Our results suggest that using a similar approach to passivation in the bulk heterojunction device structure may also be fruitful, and with such improvements, the quantum efficiency could theoretically be improved by at least a factor of 2, bringing the power conversion efficiency into the same range as that achieved in this polymer with a fullerene acceptor.

■ ASSOCIATED CONTENT

Supporting Information

Material and sample preparation along with the experimental methods description, device characteristics, quasi-steady-state photoinduced absorption and transient absorption spectra as well as details to the fitting and an alternative fitting model leading to the same conclusions. This information is available free of charge via the Internet at http://pubs.acs.org/.

■ AUTHOR INFORMATION

Corresponding Author

*E-mail: phytrptj@gmail.com (J.J.A.), ian.howard@mpip-mainz.mpg.de (I.A.H.), laquai@mpip-mainz.mpg.de (F.L.).

Author Contributions

‖These authors contributed equally to this work.

Notes

The authors declare no competing financial interest.

⊥Inquiries about surfactant and sample preparation should be addressed to J.J.A. whereas those regarding photophysics should be addressed to F.L. or I.A.H.

■ ACKNOWLEDGMENTS

M.M., C.H.L., and D.Y.Y. thank the IRTG 1404: Selforganized materials for optoelectronic devices, co-funded by the German Research Foundation (DFG) and the National Research Foundation of Korea (NRF), and the Division of Chemistry and Molecular Engineering Program of the Brain Korea 21 Project is gratefully acknowledged. M.M. also thanks the German Research Foundation (DFG) and the and the Max Planck Graduate Center (MPGC) for financial support. J.J.A. is funded by a National Science Foundation International Research Fellowship (OISE-0965057). I.P. thanks the Chemistry and Molecular Engineering Program of BK21 Project.

I.A.H. thanks the Alexander von Humboldt Foundation for a postdoctoral fellowship. F.L. thanks the Max Planck Society for funding a Max Planck Research Group.

REFERENCES

(1) Huynh, W. U.; Dittmer, J. J.; Alivisatos, A. P. Hybrid Nanorod-Polymer Solar Cells. *Science* **2002**, *295*, 2425−2427.
(2) Ren, S.; Chang, L.-Y.; Lim, S.-K.; Zhao, J.; Smith, M.; Zhao, N.; Bulović, V.; Bawendi, M.; Gradečak, S. Inorganic−Organic Hybrid Solar Cell: Bridging Quantum Dots to Conjugated Polymer Nanowires. *Nano Lett.* **2011**, 3998−4002.
(3) Seo, J.; Cho, M. J.; Lee, D.; Cartwright, A. N.; Prasad, P. N. Efficient Heterojunction Photovoltaic Cell Utilizing Nanocomposites of Lead Sulfide Nanocrystals and a Low-Bandgap Polymer. *Adv. Mater.* **2011**, 3984−3988.
(4) McDonald, S. A.; Konstantatos, G.; Zhang, S. G.; Cyr, P. W.; Klem, E. J. D.; Levina, L.; Sargent, E. H. Solution-Processed PbS Quantum Dot Infrared Photodetectors and Photovoltaics. *Nat. Mater.* **2005**, *4*, 138−142.
(5) Salafsky, J. S. Exciton Dissociation, Charge Transport, And Recombination in Ultrathin, Conjugated Polymer-TiO_2 Nanocrystal Intermixed Composites. *Phys. Rev. B.* **1999**, *59*, 10885−10894.
(6) Beek, W. J. E.; Slooff, L. H.; Wienk, M. M.; Kroon, J. M.; Janssen, R. A. J. Hybrid Solar Cells Using a Zinc Oxide Precursor and a Conjugated Polymer. *Adv. Funct. Mater* **2005**, *15*, 1703−1707.
(7) Beek, W. J. E.; Wienk, M. M.; Kemerink, M.; Yang, X.; Janssen, R. A. J. Hybrid Zinc Oxide Conjugated Polymer Bulk Heterojunction Solar Cells. *J. Phys. Chem. B* **2005**, *109*, 9505−9516.
(8) Park, I.; Lim, Y.; Noh, S.; Lee, D.; Meister, M.; Amsden, J. J.; Laquai, F.; Lee, C.; Yoon, D. Y. Enhanced Photovoltaic Performance of ZnO Nanoparticle/Poly(phenylene vinylene) Hybrid Photovoltaic Cells by Semiconducting Surfactant. *Org. Electron.* **2011**, *12*, 424−428.
(9) Shaheen, S.; Brabec, C.; Sariciftci, N.; Padinger, F.; Fromherz, T.; Hummelen, J. 2.5% Efficient Organic Plastic Solar Cells. *Appl. Phys. Lett.* **2001**, *78*, 841−843.
(10) Hindson, J. C.; Saghi, Z.; Hernandez-Garrido, J.-C.; Midgley, P. A.; Greenham, N. C. Morphological Study of Nanoparticle−Polymer Solar Cells Using High-Angle Annular Dark-Field Electron Tomography. *Nano Lett.* **2011**, *11*, 904−909.
(11) Cates, N. C.; Gysel, R.; Beiley, Z.; Miller, C. E.; Toney, M. F.; Heeney, M.; McCulloch, I.; McGehee, M. D. Tuning the Properties of Polymer Bulk Heterojunction Solar Cells by Adjusting Fullerene Size to Control Intercalation. *Nano Lett.* **2009**, *9*, 4153−4157.
(12) Westenhoff, S.; Howard, I. A.; Friend, R. H. Probing the Morphology and Energy Landscape of Blends of Conjugated Polymers with Sub-10 nm Resolution. *Phys. Rev. Lett.* **2008**, *101*, 016102.
(13) It is also possible to fix the k_i values to physically reasonable values and fit only the A_i values. Physically, the fixing of the k_i values corresponds to selecting boundaries of the volumes schematically illustrated in Figure 1, then fitting A_i values corresponds to solving for the initial population in the selected volume regions. We do this for the neat film.
(14) Yan, M.; Rothberg, L. J.; Kwock, E. W.; Miller, T. M. Interchain Excitations in Conjugated Polymers. *Phys. Rev. Lett.* **1995**, *75*, 1992−1995.
(15) Schwartz, B. J.; Hide, F.; Andersson, M. R.; Heeger, A. J. Ultrafast Studies of Stimulated Emission and Gain in Solid Films of Conjugated Polymers. *Chem. Phys. Lett.* **1997**, *265*, 327−333.
(16) Collison, C. J.; Rothberg, L. J.; Treemaneekarn, V.; Li, Y. Conformational Effects on the Photophysics of Conjugated Polymers: A Two Species Model for MEH−PPV Spectroscopy and Dynamics. *Macromolecules* **2001**, *34*, 2346−2352.
(17) Cao, Y.; Parker, I. D.; Yu, G.; Zhang, C.; Heeger, A. J. Improved Quantum Efficiency for Electroluminescence in Semiconducting Polymers. *Nature* **1999**, *397*, 414−417.
(18) Oosterhout, S. D.; Wienk, M. M.; van Bavel, S. S.; Thiedmann, R.; Koster, L. J. A.; Gilot, J.; Loos, J.; Schmidt, V.; Janssen, R. A. J. The Effect of Three-Dimensional Morphology on the Efficiency of Hybrid Polymer Solar Cells. *Nat. Mater.* **2009**, *8*, 818−824.
(19) Jianpu, W.; Baoquan, S.; Feng, G.; Greenham, N. C. Memristive Devices Based on Solution-Processed ZnO Nanocrystals. *Phys. Status Solidi A* **2010**, *207*, 484−487.
(20) Monson, T. C.; Lloyd, M. T.; Olson, D. C.; Lee, Y. J.; Hsu, J. W. P. Photocurrent Enhancement in Polythiophene- and Alkanethiol-Modified ZnO Solar Cells. *Adv. Mater.* **2008**, *20*, 4755−4759.
(21) Lloyd, M. T.; Prasankumar, R. P.; Sinclair, M. B.; Mayer, A. C.; Olson, D. C.; Hsu, J. W. P. Impact of Interfacial Polymer Morphology on Photoexcitation Dynamics and Device Performance in P3HT/ZnO Heterojunctions. *J. Mater. Chem.* **2009**, *19*, 4609−4614.
(22) Noone, K. M.; Subramaniyan, S.; Zhang, Q. F.; Cao, G. Z.; Jenekhe, S. A.; Ginger, D. S. Photoinduced Charge Transfer and Polaron Dynamics in Polymer and Hybrid Photovoltaic Thin Films: Organic vs Inorganic Acceptors. *J. Phys. Chem. C* **2011**, *115*, 24403−24410.
(23) Tang, J.; Kemp, K. W.; Hoogland, S.; Jeong, K. S.; Liu, H.; Levina, L.; Furukawa, M.; Wang, X.; Debnath, R.; Cha, D.; et al. Colloidal-Quantum-Dot Photovoltaics Using Atomic-Ligand Passivation. *Nat. Mater.* **2011**, *10*, 765−771.